Article

Macromolecular crowding modulates α-synuclein amyloid fiber growth

Istvan Horvath,[1] Ranjeet Kumar,[1] and Pernilla Wittung-Stafshede[1,*]
[1]Department of Biology and Biological Engineering, Chalmers University of Technology, Gothenburg, Sweden

ABSTRACT The crowdedness of living cells, hundreds of milligrams per milliliter of macromolecules, may affect protein folding, function, and misfolding. Still, such processes are most often studied in dilute solutions in vitro. To assess consequences of the in vivo milieu, we here investigated the effects of macromolecular crowding on the amyloid fiber formation reaction of α-synuclein, the amyloidogenic protein in Parkinson's disease. For this, we performed spectroscopic experiments probing individual steps of the reaction as a function of the macromolecular crowding agent Ficoll70, which is an inert sucrose-based polymer that provides excluded-volume effects. The experiments were performed at neutral pH at quiescent conditions to avoid artifacts due to shaking and glass beads (typical conditions for α-synuclein), using amyloid fiber seeds to initiate reactions. We find that both primary nucleation and fiber elongation steps during α-synuclein amyloid formation are accelerated by the presence of 140 and 280 mg/mL Ficoll70. Moreover, in the presence of Ficoll70 at neutral pH, secondary nucleation appears favored, resulting in faster overall α-synuclein amyloid formation. In contrast, sucrose, a small-molecule osmolyte and building block of Ficoll70, slowed down α-synuclein amyloid formation. The ability of cell environments to modulate reaction kinetics to a large extent, such as severalfold faster individual steps in α-synuclein amyloid formation, is an important consideration for biochemical reactions in living systems.

SIGNIFICANCE Proteins normally function in cells crowded by many different macromolecules. But sometimes, specific proteins begin to assemble with identical proteins into so-called amyloid fibers. Amyloid formation is a process toxic to cells that underlies many neurodegenerative diseases, for example, Parkinson's disease. To eventually find cures for such disorders, we need a molecular-mechanistic understanding of the assembly process resulting in amyloid fibers. It is not enough to investigate such reactions in dilute solutions in test tubes, one must also consider potential effects caused by the crowded cell milieu. Here, we use biophysical methods to reveal that macromolecular crowding, mimicking steric restrictions in cells, accelerate individual steps and promote secondary nucleation in the amyloid formation process of the Parkinson's disease protein α-synuclein.

INTRODUCTION

The intracellular environment is highly crowded, with an estimate of up to 400 mg/mL macromolecules (proteins, lipids, and polysaccharides), corresponding to a volume occupancy of up to 40% (1,2). High concentrations of macromolecules restrict the available molecular space by their mutual impenetrability and repulsive interactions, often termed excluded-volume effect. The excluded-volume effect is accompanied by increased opportunities for nonspecific (chemical or "soft") interactions, increased (heterogeneous) viscosity, reduced macromolecule dynamics, as well as changes in solvent polarity and water activity, which in total describe the macromolecular crowding effect (3,4). The excluded-volume effect is an entropic force in which (because of steric restrictions) compact and assembled protein species are favored (1,5–8). Many in vitro studies of excluded-volume effects using so-called macromolecular crowding agents, for example, the inert sugar-based polymers Ficoll and dextran (4,9), on protein folding and stability have shown increased folded-state stability and slower unfolding reactions in the presence of macromolecular crowding agents (9–12). Macromolecular crowding typically favors protein-protein interactions because assembled states will reduce the volume occupancy and number of species in solution. However, the effect on reaction kinetics will depend on conformational changes and rate-limiting steps. Here, amyloid formation is interesting because this assembly process involves multiple steps and protein-conformational changes (13). Amyloid fibrils are biological polymers composed of

monomeric protein units noncovalently assembled through β-strands arranged perpendicularly to the fibril axis, thereby forming a cross-β structure (14). Many proteins can form amyloid fibrils at certain solvent conditions (13), but this process is mostly connected to human diseases such as Alzheimer's disease and Parkinson's disease (PD) (15–17).

PD is the second most common neurodegenerative disorder and the most frequent movement disorder today and there is only symptomatic treatment (18,19). Assembly of the protein α-synuclein (aS) into amyloid fibrils has been linked to the molecular basis of PD, with aS amyloids being the major content of pathological neuronal inclusions, the Lewy bodies, found in PD patient brain cells (20–22). In accord, duplications, triplications, and point mutations in the aS gene are linked to familial PD cases (23). In solution, aS is an intrinsically disordered polypeptide, but it adopts significant α-helical structure when interacting with lipid vesicles. Despite the key role of aS in PD, its exact functions remain unknown but appear related to synaptic vesicle release and trafficking, regulation of enzymes and transporters, and control of the neuronal apoptotic response (24–26). Amyloid formation aS (and other amyloidogenic proteins) proceeds via at least two reaction steps: primary nucleation and elongation of fibrils (14,27). The process is, in addition, typically catalyzed by secondary processes including secondary nucleation (14,27) and, in some cases, fibril fragmentation (28). It is reported that for aS, primary processes dominate at physiological pH, whereas at lower pH, secondary processes become more important (29).

To eventually cure or prevent PD, we need to understand how and when aS amyloid formation takes place in its natural environment in vivo. A first step toward this is to determine the effects of macromolecular crowding on the aggregation process of aS in vitro. To date, however, most aS amyloid formation studies are performed in diluted buffer solutions. We here addressed this knowledge gap by carefully probing the effects of excluded volume on the molecular steps involved in aS amyloid formation. To create excluded-volume conditions, we have used the macromolecular crowding agent Ficoll70 (70 kDa), which is a sucrose-based branched polymer often used for this purpose (30,31). Although there may be exceptions (32), Ficoll70 has been shown to only provide steric, excluded-volume effects without chemical interactions with proteins (9,12,33). In contrast to earlier reports of crowding effects on aS aggregation (34–38), we have characterized the excluded-volume effect on fiber-seeded experiments to eliminate issues with shaking and glass beads.

MATERIALS AND METHODS

Materials

Human aS was expressed and purified as described in (39). Molecular biology grade Ficoll70 (Sigma-Aldrich, St. Louis, MO) stock solutions were prepared in Tris-buffered saline (TBS; 0.05 M Tris-HCl buffer (pH 7.6 (pH 7.4 at 37°C)) with 0.15 M NaCl, 93318; Sigma-Aldrich) buffer,

the pH of the solution was adjusted to 7.6 after the Ficoll70 was dissolved. All solutions used were cleared with 0.22-μm filtering.

Amyloid formation

Before aS aggregation assays, size-exclusion chromatography was performed on freshly thawed aS protein solutions using a Superdex 75 10/300 (Cytiva, Uppsala, Sweden) gel filtration column in TBS buffer to ensure that the starting material was monomeric. The aggregation assay in shaking conditions were conducted as described previously (40,41): aS amyloid formation reactions were conducted in 96-well, half-area transparent-bottom plates with a nonbinding surface (CLS3881; Corning, Corning, NY) with one 2-mm glass bead in each well using a plate reader and incubator instrument (Fluorostar Optima; BMG Labtech, Ortenberg, Germany). Measurements were performed in TBS (pH 7.4) with 0.15 M NaCl buffer in the presence of 20 μM Thioflavin T (ThT; T3516; Sigma-Aldrich), 2 mM EDTA, and 0.005% sodium azide at 37°C using 200 rpm agitation for 5 min during 20-min measurement cycles; fluorescence was measured from the bottom side of the plate, and the aS concentration was 50 μM. For measurements in quiescent conditions, the 5-min agitation was omitted from the protocol, and no glass beads were used in the wells. Samples were typically incubated for 120 h, and fluorescence was measured every 20 min. ThT was excited at 440 nm, and emission was recorded at 480 nm. All ThT-containing aS aggregation experiments were performed in quadruplicate at each time (on the same plate), and the experiments were repeated three independent times (different plates).

aS seed preparation

Amyloid fiber seeds of aS were prepared by incubating 250 μM aS in TBS with 5% premade fibrils (prepared using agitation in plate reader as described in the aggregation assays) for 1 week at 37°C. To obtain short fiber seeds, an aggregated sample was sonicated for 10 s using a probe sonicator (stepped microtip and Ultrasonic Processor Sonics Vibra-Cell; Sonics & Materials, Newtown, CT) at an amplitude of 20% and an alternating cycle of 5 s on and 5 s off. The aggregated material was characterized by atomic force microscopy (AFM) showing long amyloid fibers (>5 μm) for the nonsonicated and short amyloid fibers (<1 μm) for the sonicated protein samples. The fiber seed solutions were aliquoted, flash frozen in liquid nitrogen, and stored in −150°C until usage.

AFM

Samples from aggregation reactions were diluted into Milli-Q water (10–20 times; MilliporeSigma, Burlington, MA) and deposited on freshly cleaved mica. After 10 min, the mica was rinsed with filtered Milli-Q water (MilliporeSigma) and dried under a gentle nitrogen stream. Images were recorded on an NTEGRA Prima setup (NT-MDT, Moscow, Russia) using a gold-coated single crystal silicon cantilever (NT-MDT, NSG01, spring constant of ∼5.1 N/m) and a resonance frequency of ∼180 kHz. Here, 512 × 512-pixel images were acquired with a 0.5-Hz scan rate. Images were analyzed using the WSxM 5.0 software. For each sample, images were taken in at least three different 50 × 50-μm areas; the images shown in the figures are representatives for each sample. For the analysis of the oligomer sizes, flooding analysis was used; particles larger than 2 nm were included in the analysis.

Circular dichroism spectroscopy

Far-UV circular dichroism (CD) spectra of aS (5 μM) were recorded on a Chirascan spectropolarimeter (Applied PhotoPhysics, Leatherhead, UK) in 10 mM phosphate buffer in the absence and presence of Ficoll70. CD spectra between 250 and 190 nm were collected in a quartz cuvette (path

length of 1 mm) with a bandwidth of 1 nm, a step size of 1 nm, and a scanning speed of 50 nm/min. Three individual spectra were acquired and averaged for each condition. The CD spectra of the respective Ficoll70 solutions were subtracted from the spectra measured on the protein.

Kinetic data analysis

All fluorescence data were normalized before analysis. For the determination of the initial rates in seeded (with sonicated seeds) conditions, linear fits were applied to fluorescence data points in the first 1–2 h of the aggregation reactions (before curvature was noted). Reaction half-times were determined as the time point in which the fluorescence signal exceeded 0.5 (i.e., halfway to maximal intensity) in the normalized ThT data. For analysis of seeded reactions (sonicated seeds, initial rates; nonsonicated seeds, half-times), data from 12 individual replicates (four replicas performed in three independent experiments) were averaged (except for 2.5, 5, and 20% seeds in 280-mg/mL Ficoll70 conditions in which only nine replicates were used for the averages). Error bars denote standard deviation in the initial rate and half-time plots, considering all replicates at each condition.

Viscosity measurements

The bulk (macro)viscosities of Ficoll70 and sucrose solutions were determined using a Discovery HR-3 rheometer from TA Instruments (New Castle, DE). The geometry was a cone plate with a 40-mm diameter, one-degree angle, and 26 μm of a gap. The viscosity was recorded at T = 37°C between shear rates of 0.01 and 1000 s^{-1}. The temperature was controlled using a Peltier plate. The viscosity profiles showed a Newtonian profile (as expected for this sort of samples) with viscosity values of 3.91 $\pm$ 0.07 cP for 140 mg/mL Ficoll 70, 17.6 $\pm$ 2.28 cP for 280 mg/mL Ficoll70, and 4.19 $\pm$ 0.15 cP for 550 mg/mL sucrose.

RESULTS AND DISCUSSION
Shaking conditions not useful

Aggregation of aS into amyloid fibers in vitro is often probed using monomeric aS that is placed at 37°C in a plate reader with shaking and glass beads to speed up the reaction. At these conditions, aS amyloid formation, monitored in real time by ThT fluorescence, shows a sigmoidal curve in which there is first a lag time, followed by a growth phase at around 20 h (for 50 μM), and then a plateau is reached. Initial experiments, adding Ficoll70 to such reactions, revealed that this is not a useful setup for crowding experiments. Because Ficoll70 increases the viscosity, it will affect the movement of the glass beads. We found that at very high Ficoll70 (280 mg/mL), aS aggregation appeared faster, but at lower Ficoll70 (140 mg/mL), aggregation of aS was reduced, as compared with in buffer, with this experimental setup (Fig. S1). To avoid the issues with shaking and glass beads, we turned to quiescent conditions without glass beads. At nonshaking conditions, aS on its own will not aggregate within our typical experimental time frame of up to 140 h. However, by the addition of amyloid fiber seeds, the slow primary nucleation is bypassed, and amyloid formation is detected immediately (see below).

Effect of Ficoll70 on nonseeded amyloid formation reaction

The presence of Ficoll70 does not affect the disordered far-UV CD signal of aS monomers in solution (Fig. S1 D). At conditions without shaking (and in the absence of amyloid seeds), we find that the presence of Ficoll70 (70–350 mg/mL tested) can trigger aS amyloid formation (Fig. S2). The presence of less than 140 mg/mL Ficoll70 did not increase the ThT fluorescence, whereas 210 mg/mL was enough to obtain a completed aggregation curve within 160 h. Interestingly, increasing the Ficoll70 concentration to 350 mg/mL did not decrease the lag time as compared with aS samples containing 280 mg/mL Ficoll70. We selected 140 and 280 mg/mL Ficoll70 as our conditions for further studies as they span from the lower to the higher end of the crowdedness in vivo (42). Both these Ficoll70 concentrations trigger aggregation of aS monomers within the time frame of the experiment (only partly for 140 mg/mL) (Fig. 1 A). The resulting amyloid fibers formed at these conditions look like amyloids of aS formed in buffer condition when analyzed by AFM (Fig. 1, B and C); Ficoll70 itself is too small to be visible by AFM, and only some aggregates can be detected when analyzing Ficoll70 samples by AFM (Fig. 1 D). The time to 50% change in ThT fluorescence (midpoint of transition) with 280 mg/mL Ficoll70 is ∼25 h, and the ThT fluorescence starts to rise at around 14–15 h. For the 140 mg/mL Ficoll70 condition, the ThT fluorescence starts to rise at ∼50 h. If this is compared with buffer conditions in which no ThT fluorescence change is detected during 140 h, it implies that the overall aS aggregation reaction in the presence of 280 mg/mL Ficoll is at least 10-fold faster than in buffer. Likely, the accelerating factor by 280 mg/mL Ficoll70 is larger than 10-fold because a transition midpoint of 400 h was reported in another study of aS aggregation in buffer (43). In that study, a 14 times higher protein concentration was used (no shaking and beads, no seeds, and high salt) compared with here. Notably, we found a similar accelerating effect when including another crowding agent, polyethylene glycol 35 (35 kDa), but the addition of Ficoll's building block, the small-molecule osmolyte sucrose, which provides increased viscosity and solvation effects but not increased excluded volume, had no initiation of aS amyloid formation within 100 h (Fig. S3).

Effect of Ficoll70 on primary nucleation

The accelerated aggregation curves in the presence of Ficoll 70 may be explained by excluded-volume effects on all or some of the microscopic processes, with primary nucleation, elongation, and secondary nucleation as most important, that take place during amyloid formation. To test if the presence of Ficoll70 accelerates aS primary nucleation, we analyzed samples from aggregation reactions after 4 h of incubation in buffer and 280 mg/mL Ficoll70 conditions. At
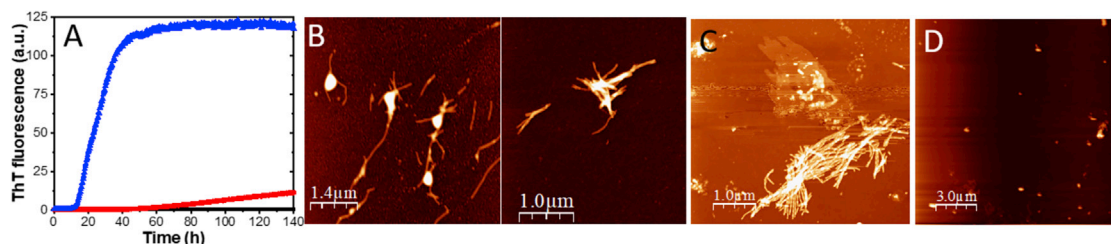
FIGURE 1 Effect of Ficoll70 on aS amyloid formation at quiescent conditions. (*A*) Amyloid formation kinetics (curves are averages of four individual replicates) of aS in quiescent conditions as followed by ThT fluorescence in buffer (*black*) in the presence of 140 mg/mL (*red*) and in the presence of 280 mg/mL Ficoll70 (*blue*) (examples of individual traces shown in Fig. S6 *A*). (*B*) AFM of aS amyloid fibers formed in the presence of 280 mg/mL Ficoll70, (*C*) AFM of aS amyloid fibers formed in buffer with agitation, and (*D*) AFM of 280 mg/mL Ficoll70 alone.

this time point, both curves remain flat with respect to ThT signal; thus, it is a data point in the lag phase. AFM analysis of these solutions showed that the Ficoll70 sample contained spherical oligomers with sizes of 5–7 nm, whereas no oligomers were found in the aS sample in buffer (Fig. S4, *A–C*). Notably, the few aggregates sometimes detected by AFM in Ficoll70-only solutions are larger (>20 nm) and do not match the spherical species detected in the presence of aS (Figs. 1 *D* and S4 *D*). CD analysis of 4-h samples with crowding reveals that these aS assemblies have unstructured secondary structure (Fig. S4 *E*). Therefore, these aS species are likely intermediates in the primary nucleation step, which eventually convert to β-structured seeds that can be elongated. Taken together, the presence of the macromolecular crowding agent Ficoll70 accelerates the nonseeded (overall) aS amyloid formation reaction, which appears to include enhancement of primary nucleation because oligomers are detected at early time points.

Effect of Ficoll70 on amyloid fiber elongation

To specifically investigate aS amyloid fiber elongation, we turned to fiber-seeded reactions using sonicated fiber seeds. Sonication of preformed fibers gives shorter amyloid fibers, thus with more ends to elongate (per concentration of aS monomers) as compared with nonsonicated fibers. AFM of sonicated seeds are shown in Fig. 2 *D*, and size analysis gives an average seed length of ∼200 nm (Fig. S5). In Fig. 2, *A–C*, we show ThT aggregation data for aS-seeded reactions at different concentrations of sonicated seeds comparing no added Ficoll70 (i.e., buffer), 140- and 280-mg/mL Ficoll70 conditions. Examples of sets of replicate curves are shown in Fig. S6 for both seeded and unseeded reactions, implying high reproducibility. As expected for fiber-seeded aggregation reactions, the lag phase is bypassed, and elongation starts immediately in these experiments. Fiber seed concentration is given in molar percent of monomers present as fiber seeds versus monomers free in solution. It is clear from the data that fiber-seeded reactions are also accelerated by the presence of Ficoll70, but the effect is not as extensive as the effect on the nonseeded amyloid formation reaction

(cf. Fig. 1 *A*). Whereas the kinetic traces at 20% fiber seed all show hyperbolic shapes, at a lower percentage of seeds, the kinetic traces in the crowded solutions appear biphasic with a second phase that starts around 5–8 h of reaction. Thus, the reaction mechanism differs between low and high seed percentages. Two-phase behavior can be an indication of secondary processes taking over when enough elongation has taken place (44) and will be discussed in the next section.

To analyze the elongation process in a quantitative way, we collected aggregation data for four amyloid seed concentrations at 0, 140, and 280 mg/mL Ficoll70 at a fixed aS monomer concentration (Fig. 2, *E–G*). Analysis of the initial rates (slope in the first 1–2 h, shown in Fig. S7) provides a measure of the elongation rate at that condition. In Fig. 2 *H*, we plot the initial rates versus amyloid fiber seed concentration for the three different conditions, and each data set is fitted to a linear dependence. A linear dependence between initial rates and seed concentrations is expected for processes involving elongation (44). It is clear from the plot that in the presence of crowding agent, initial rates are faster at each seed concentration (by a factor of ∼2). Also, the dependence of the initial rate on the seed concentration is stronger (i.e., steeper slopes of fitted lines) with the presence of crowding agent, although the 140- and 280-mg/mL Ficoll70 data are rather similar to each other. The increased slope for crowded conditions means that each unit of new fiber seed added will have a larger effect on the aggregation kinetics when in a crowded condition. As another way to showcase the difference between the conditions, to get the same enhancing effect on elongation kinetics, one needs to add 10% seeds in buffer but only 3–4% fiber seeds in crowded conditions. This implies that in vivo, which is a crowded condition, a small number of seeds will have a larger effect on its surrounding polypeptides than what is measured in buffer. We speculate this to be relevant for disease onset in patients. In agreement with our results, the single existing publication that describes macromolecular crowding effects on aS fiber elongation reported (using quartz crystal microbalance experiments) that the elongation rate was increased by 1.8-fold in the presence of 50 mg/mL dextran (200 kDa) (45).
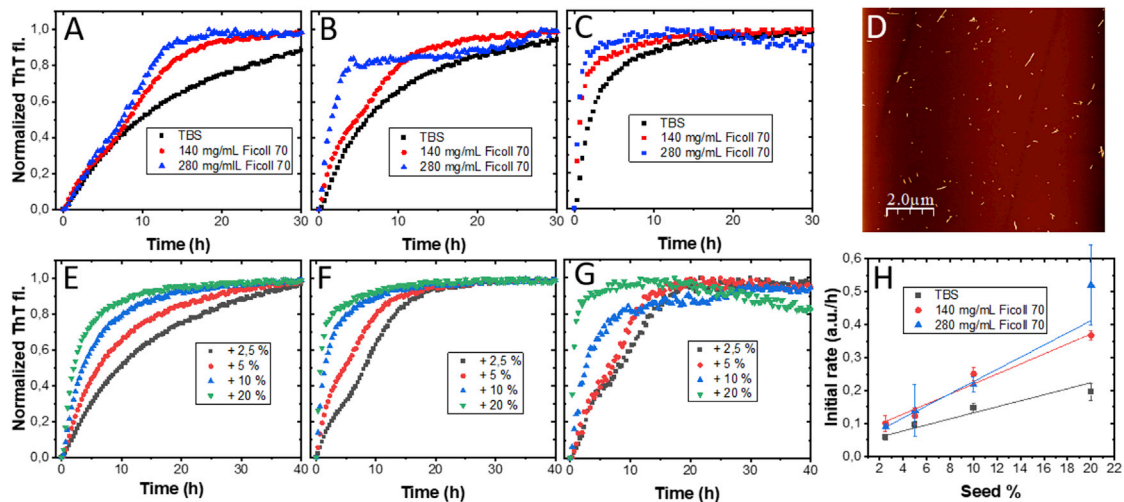
FIGURE 2 Effects of sonicated seeds on aS amyloid formation. Seeded amyloid formation kinetics with and without added Ficoll70 with 2.5 (*A*), 5 (*B*), and 20% (*C*) preformed sonicated aS amyloid fibers. (*D*) AFM image of sonicated amyloid fibers used in the measurements. Shown are seeded aggregation curves with various fiber seed concentrations in buffer (*E*), in 140 mg/mL (*F*), and in 280 mg/mL Ficoll70 (*G*). The traces in (*A*)–(*C*) are replotted in (*E*)–(*G*) together with 10% seed data. All traces shown are representative individual traces. In Fig. S6, we show sets of individual traces for some different conditions to illustrate the magnitude of variability in the kinetic data. (*H*) Plot of initial rates of fiber elongation, as determined by linear fitting of the first 1–2 h of the reaction at each condition (Fig. S7 for examples of such data), versus molar percent seeds. Initial rates derived from individual experiments (between 9 and 12 for each condition) were then averaged and is here plotted with standard deviation. The average initial rate versus seed concentration (given as molar percent monomers in added seeds versus monomers in solution) at each solution condition was fitted to a linear equation (*solid lines*). Monomeric aS concentration was 50 μM in all experiments.

For comparison, we performed similar aS amyloid fiber (sonicated seeds) seeding experiments in the presence of sucrose at a high concentration (Fig. S8). In contrast to in Ficoll70, we found seeded aS amyloid formation reactions in the presence of sucrose to be slowed down as compared with in buffer. The elongation rates were two to three times slower with sucrose as compared with without. The viscosity of 550 mg/mL sucrose ($\sim$4 cP) match the bulk viscosity of 140 mg/mL Ficoll70, but whereas the micro- and macro-viscosities are the same in sucrose, for Ficoll70, the micro-viscosity is lower than the bulk viscosity (46). In accord with the sucrose effect on aS elongation here, we previously showed that sucrose retarded amyloid fiber elongation kinetics of the amyloidogenic protein parvalbumin (47).

Effect of Ficoll70 on secondary pathways

ThT kinetic data collected for amyloid-fiber-seeded reactions within a time frame in which there is no detectable reaction without added seed cannot include primary nucleation but may involve secondary processes in addition to elongation (48,49). Observation of biphasic behavior at such conditions, in which there is a first phase (at early time points) that transitions to another kinetic phase (at later time points), in the ThT kinetics must include secondary processes. In principle, when enough elongation has occurred in a sample, secondary (faster) processes take over the reaction (44). For aS aggregation, this behavior may be favored in seeded reactions using nonsonicated seeds for which the number of fiber ends are fewer than

when adding sonicated seeds (cf. Fig. 2 *D*, sonicated seeds; Fig. 3 *D*, nonsonicated seeds). Like with the sonicated seeds (Fig. 2), the addition of nonsonicated seeds to aS monomeric samples removes the lag time at all conditions (buffer and Ficoll70). In Fig. 3 *A*, for aS aggregation upon addition of nonsonicated seeds in buffer, most kinetic curves are hyperbolic, indicating no secondary processes and only elongation. However, at the lowest seed percentage (2.5%), a tendency for biphasic behavior is noted in the kinetics trace. In the presence of a crowding agent, 140 and 280 mg/mL Ficoll 70, the biphasic behavior is evident at all conditions except at the highest seed percentage (20%; here, hyperbolic curve) (Fig. 3, *B and C*). Inspection of Fig. 2, *F and G* shows that also for sonicated fiber seeds at low concentrations, the kinetic traces are biphasic in the presence of crowding agent. Importantly, there are no primary nucleation within 140, 50, and 15 h for buffer, 140 and 280 mg/mL Ficoll70 conditions, respectively, based on Fig. 1 *A*. Thus, the kinetics detected are due to the added seeds only and, when biphasic, must include an additional process in addition to elongation. Secondary processes can involve secondary nucleation, meaning new fibers are nucleated on the surface of existing fibers, and fragmentation, meaning existing fibers break forming new fiber ends that can be elongated (48,49). The latter process (fragmentation) is likely not important here because we have quiescent conditions.

According to closed-form analytical solutions to rate equations for filament assembly via elongation and secondary pathways (50,51), a plot of the time to midpoint of transition versus the logarithm of the seed concentration should
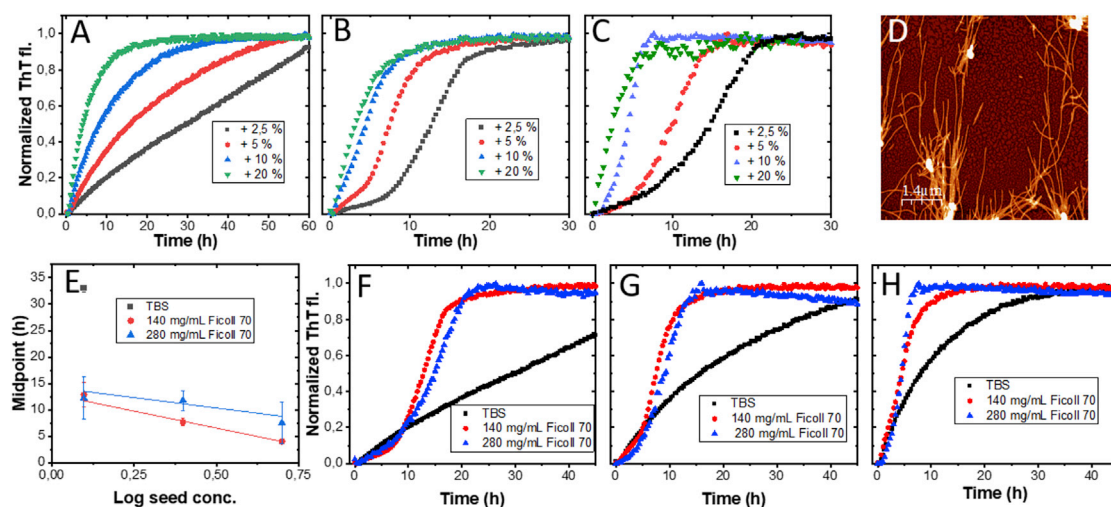
FIGURE 3 Effects of nonsonicated seeds on aS amyloid formation. Shown is seeded aggregation with nonsonicated aS fibers in TBS (*A*), in 140 mg/mL Ficoll 70 (*B*), and in 280 mg/mL Ficoll 70 (*C*). (*D*) AFM image of the nonsonicated fibers used in the measurements. (*E*) Plot of time to midpoint of ThT transition versus the logarithm of seed concentration at different Ficoll70 concentrations (individual kinetic traces (~12 replicates) for each condition was here averaged; average shown with standard deviation). The midpoints versus logarithm (seed concentration) for the two Ficoll70 conditions were fitted to linear equations (excluding 20% seed data because it is not biphasic) shown as solid lines. For TBS, only the midpoint for 2.5% seeds is included because it is the only curve that shows some content of secondary nucleation. Shown are the comparing aggregation curves in TBS, 140 and 280 mg/mL Ficoll70 at 2.5 (*F*), 5 (*G*), and 10% (*H*) nonsonicated seeds (kinetic curves from *A–C* panels are replotted). Monomeric aS concentration was 50 μM at each condition. All aggregation curves shown in (*A–C*) and (*F–H*) are representative single measurements (each taken from 12 replicates collected at each condition).

show a linear dependency. As can be seen, such a dependence appears reasonable for the crowded conditions (Fig. 3 *E*). We therefore propose that the presence of macromolecular crowding promotes secondary processes during aS aggregation at pH 7, quiescent conditions. Inspection of Fig. 3 *E* reveals that the difference in midpoints between the buffer (at 2.5% seeds, in which biphasic behavior is observed; data point (*black square*) is next to the E label in the panel) and crowded conditions, is around threefold, i.e., secondary processes are accelerated by a factor 3 at crowded conditions. AFM and far-UV CD analysis of aS amyloid fibers formed in the presence of nonsonicated seeds reveal no major differences in amyloid fiber morphology or β-sheet secondary structure as compared with fibers formed with sonicated fiber seeds in both buffer and Ficoll70 (Fig. S9).

Clear biphasic behavior, indicating contributions from secondary nucleation, is also found in the seeded (sonicated seeds) reactions in the presence of sucrose (Fig. S8). The underlying reason for this stimulation of secondary processes by both Ficoll70 and sucrose (although one agent speeds up and the other slows down overall reaction) need further investigation.

When the data with nonsonicated seeds are plotted at fixed seed concentration versus crowding agent concentration variation, it emerges that the difference between 140 and 280 mg/mL Ficoll70 is small at each percent seed condition (Fig. 3, *F–H*). This implies that the accelerating effect on aS assembly kinetics approaches saturation at high Ficoll70 concentrations; this may be due to Ficoll70-induced viscosity effects (slowing translational diffusion) counter-

acting further excluded-volume-induced acceleration at high Ficoll70 concentrations.

CONCLUSIONS

We have here analyzed the effect of one macromolecular crowding agent (Ficoll70) on individual steps involved in aS amyloid formation kinetics at quiescent conditions using seeding. We used 140 and 280 mg/mL Ficoll70 here, which is comparable with the estimates of macromolecules in the cytoplasm of cells that range between 5 and 400 mg/mL (10,52). A recent study suggested that 150–200 mg/mL Ficoll70 match the condition in the cytoplasm with respect to translational and rotational diffusion (42). Nonetheless, whereas in vitro crowding experiments are homogeneous, cellular conditions will be very heterogeneous. In accord with the overall conclusions of earlier work (34–38), aS amyloid formation is accelerated in the presence of macromolecular crowding agents in vitro. However, our approach contrasts the earlier studies (34–38) that either used shaking and bead conditions or quiescent conditions without seeds in that it makes possible the analysis of individual processes. From our collected results, we can conclude that primary nucleation, fiber elongation as well as secondary nucleation are accelerated by the macromolecular crowding agent Ficoll70. Thus, introduction of excluded-volume results in faster microscopic processes but no change of underlying amyloid formation mechanism (Fig. 4).

Although quantification is difficult, the data suggest that primary nucleation is more affected by macromolecular crowding than elongation and secondary nucleation steps.
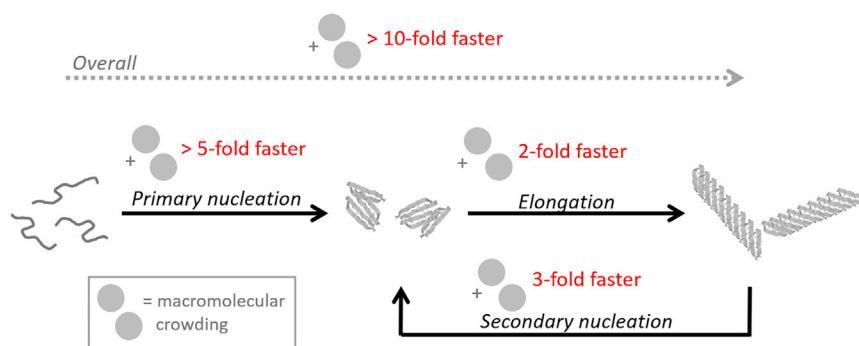
FIGURE 4 Illustration of macromolecular crowding effects on aS amyloid formation as determined in this study using Ficoll70 as crowding agent (pH 7; quiescent conditions). We note that the acceleration factors (in *red*) are estimates. Based on aggregation experiments without amyloid seeds, the overall reaction is accelerated at least 10-fold (Fig. 1 *A*). Concentration-dependent analysis of elongation specifically (Fig. 2 *H*) reveals a twofold increase with crowding agent; this implies that primary nucleation must be accelerated at least fivefold (to get a net effect that is larger than 10-fold). Secondary nucleation is stimulated with Ficoll70 and at conditions in which this is seen in part also in buffer (2.5% nonsonicated seeds Fig. 3 *E*; typically, there is very little secondary nucleation in buffer at neutral pH); the reaction is ~3-fold faster in Ficoll70 than in buffer.

This implies that the reduction of excluded volume is larger for initial oligomer formation and nucleation than for the addition of monomers to growing fiber ends. Nonetheless, alterations of biochemical reactions by modest factors, such as 2 or 3, may still have dramatic effects in vivo. This study is only a first step to dissect macromolecular crowding effects on amyloid fiber formation reactions. Further studies including other crowding agents, mixtures of crowding agents, and other amyloidogenic proteins are required to reveal general features. Finally, a note of caution. Our initial data using shaking in the presence of glass beads suggest that such conditions are not appropriate (because of viscosity effects on bead movement) for macromolecular crowding experiments.

SUPPORTING MATERIAL

Supporting material can be found online at https://doi.org/10.1016/j.bpj.2021.06.032.

AUTHOR CONTRIBUTIONS

I.H. and P.W.-S. designed the study. I.H. and R.K. performed the experiments. I.H. and P.W.-S. analyzed the data. I.H. and P.W.-S. wrote the article.

ACKNOWLEDGMENTS

REFERENCES

1. Kuznetsova, I. M., K. K. Turoverov, and V. N. Uversky. 2014. What macromolecular crowding can do to a protein. *Int. J. Mol. Sci.* 15:23090–23140.

2. Ellis, R. J., and A. P. Minton. 2003. Cell biology: join the crowd. *Nature.* 425:27–28.

3. Davis, C. M., and M. Gruebele. 2018. Non-steric interactions predict the trend and steric interactions the offset of protein stability in cells. *ChemPhysChem.* 19:2290–2294.

4. Gao, M., and R. Winter. 2015. The effects of lipid membranes, crowding and osmolytes on the aggregation, and fibrillation propensity of human IAPP. *J. Diabetes Res.* 2015:849017.

5. Ralston, G. B. 1990. Effects of crowding in protein solutions. *J. Chem. Educ.* 67:857–860.

6. van den Berg, B., R. J. Ellis, and C. M. Dobson. 1999. Effects of macromolecular crowding on protein folding and aggregation. *EMBO J.* 18:6927–6933.

7. Minton, A. P. 2005. Models for excluded volume interaction between an unfolded protein and rigid macromolecular cosolutes: macromolecular crowding and protein stability revisited. *Biophys. J.* 88:971–985.

8. Minton, A. P. 2001. The influence of macromolecular crowding and macromolecular confinement on biochemical reactions in physiological media. *J. Biol. Chem.* 276:10577–10580.

9. Christiansen, A., and P. Wittung-Stafshede. 2014. Synthetic crowding agent dextran causes excluded volume interactions exclusively to tracer protein apoazurin. *FEBS Lett.* 588:811–814.

10. Ellis, R. J. 2001. Macromolecular crowding: obvious but underappreciated. *Trends Biochem. Sci.* 26:597–604.

11. van den Berg, B., R. Wain, …, R. J. Ellis. 2000. Macromolecular crowding perturbs protein refolding kinetics: implications for folding inside the cell. *EMBO J.* 19:3870–3875.

12. Christiansen, A., and P. Wittung-Stafshede. 2013. Quantification of excluded volume effects on the folding landscape of *Pseudomonas aeruginosa* apoazurin in vitro. *Biophys. J.* 105:1689–1699.

13. Chiti, F., and C. M. Dobson. 2017. Protein misfolding, amyloid formation, and human disease: a summary of progress over the last decade. *Annu. Rev. Biochem.* 86:27–68.

14. Chiti, F., and C. M. Dobson. 2017. Protein misfolding, amyloid formation, and human disease: a summary of progress over the last decade. *In* Annual Review of Biochemistry, *Vol. 86.* R. D. Kornberg, ed.. Annual Reviews, pp. 27–68.

15. Jarrett, J. T., E. P. Berger, and P. T. Lansbury, Jr. 1993. The carboxy terminus of the beta amyloid protein is critical for the seeding of amyloid formation: implications for the pathogenesis of Alzheimer's disease. *Biochemistry.* 32:4693–4697.

16. Wakabayashi, K., K. Matsumoto, …, H. Takahashi. 1997. NACP, a presynaptic protein, immunoreactivity in Lewy bodies in Parkinson's disease. *Neurosci. Lett.* 239:45–48.

17. Cooper, G. J., A. C. Willis, …, K. B. Reid. 1987. Purification and characterization of a peptide from amyloid-rich pancreases of type 2 diabetic patients. *Proc. Natl. Acad. Sci. USA.* 84:8628–8632.

18. John, A., and W. van der Pluijm. 2018. The global prevalence of Parkinson's disease over the next ten years. *Ann. Neurol.* 84:S219.

19. Elkouzi, A., V. Vedam-Mai, ..., M. S. Okun. 2019. Emerging therapies in Parkinson disease - repurposed drugs and new approaches. *Nat. Rev. Neurol.* 15:204–223.

20. Goldberg, M. S., and P. T. Lansbury, Jr. 2000. Is there a cause-and-effect relationship between alpha-synuclein fibrillization and Parkinson's disease? *Nat. Cell Biol.* 2:E115–E119.

21. Spillantini, M. G., M. L. Schmidt, ..., M. Goedert. 1997. α-synuclein in Lewy bodies. *Nature.* 388:839–840.

22. Uversky, V. N. 2007. Neuropathology, biochemistry, and biophysics of α-synuclein aggregation. *J. Neurochem.* 103:17–37.

23. Polymeropoulos, M. H., C. Lavedan, ..., R. L. Nussbaum. 1997. Mutation in the α-synuclein gene identified in families with Parkinson's disease. *Science.* 276:2045–2047.

24. Fusco, G., T. Pape, ..., A. De Simone. 2016. Structural basis of synaptic vesicle assembly promoted by α-synuclein. *Nat. Commun.* 7:12563.

25. Dev, K. K., K. Hofele, ..., H. van der Putten. 2003. Part II: α-synuclein and its molecular pathophysiological role in neurodegenerative disease. *Neuropharmacology.* 45:14–44.

26. Lassen, L. B., L. Reimer, ..., P. H. Jensen. 2016. Protein partners of α-synuclein in health and disease. *Brain Pathol.* 26:389–397.

27. Meisl, G., J. B. Kirkegaard, ..., T. P. J. Knowles. 2016. Molecular mechanisms of protein aggregation from global fitting of kinetic models. *Nat. Protoc.* 11:252–272.

28. Bolognesi, B., S. I. A. Cohen, ..., L. M. Luheshi. 2014. Single point mutations induce a switch in the molecular mechanism of the aggregation of the Alzheimer's disease associated Aβ42 peptide. *ACS Chem. Biol.* 9:378–382.

29. Buell, A. K., C. Galvagnion, ..., C. M. Dobson. 2014. Solution conditions determine the relative importance of nucleation and growth processes in α-synuclein aggregation. *Proc. Natl. Acad. Sci. USA.* 111:7671–7676.

30. Wang, Y., H. He, and S. Li. 2010. Effect of Ficoll 70 on thermal stability and structure of creatine kinase. *Biochemistry (Mosc.).* 75:648–654.

31. Zhou, H. X., G. Rivas, and A. P. Minton. 2008. Macromolecular crowding and confinement: biochemical, biophysical, and potential physiological consequences. *Annu. Rev. Biophys.* 37:375–397.

32. Nasreen, K., Z. A. Parray, ..., A. Islam. 2020. Interactions under crowding milieu: chemical-induced denaturation of myoglobin is determined by the extent of heme dissociation on interaction with crowders. *Biomolecules.* 10:E490.

33. Christiansen, A., Q. Wang, ..., P. Wittung-Stafshede. 2010. Factors defining effects of macromolecular crowding on protein stability: an in vitro/in silico case study using cytochrome c. *Biochemistry.* 49:6519–6530.

34. Uversky, V. N., E. M Cooper, ..., A. L. Fink. 2002. Accelerated alpha-synuclein fibrillation in crowded milieu. *FEBS Lett.* 515:99–103.

35. Biswas, S., A. Bhadra, ..., I. Roy. 2021. Molecular crowding accelerates aggregation of α-synuclein by altering its folding pathway. *Eur. Biophys. J.* 50:59–67.

36. Munishkina, L. A., E. M. Cooper, ..., A. L. Fink. 2004. The effect of macromolecular crowding on protein aggregation and amyloid fibril formation. *J. Mol. Recognit.* 17:456–464.

37. Munishkina, L. A., A. Ahmad, ..., V. N. Uversky. 2008. Guiding protein aggregation with macromolecular crowding. *Biochemistry.* 47:8993–9006.

38. Shtilerman, M. D., T. T. Ding, and P. T. Lansbury, Jr. 2002. Molecular crowding accelerates fibrillization of alpha-synuclein: could an increase in the cytoplasmic protein concentration induce Parkinson's disease? *Biochemistry.* 41:3855–3860.

39. Werner, T., R. Kumar, ..., P. Wittung-Stafshede. 2018. Abundant fish protein inhibits α-synuclein amyloid formation. *Sci. Rep.* 8:5465.

40. Horvath, I., and P. Wittung-Stafshede. 2016. Cross-talk between amyloidogenic proteins in type-2 diabetes and Parkinson's disease. *Proc. Natl. Acad. Sci. USA.* 113:12473–12477.

41. Horvath, I., C. F. Weise, ..., P. Wittung-Stafshede. 2012. Mechanisms of protein oligomerization: inhibitor of functional amyloids templates α-synuclein fibrillation. *J. Am. Chem. Soc.* 134:3439–3444.

42. Yamamoto, J., A. Matsui, ..., M. Kinjo. 2021. Quantitative evaluation of macromolecular crowding environment based on translational and rotational diffusion using polarization dependent fluorescence correlation spectroscopy. *Sci. Rep.* 11:10594.

43. Yagi, H., E. Kusaka, ..., Y. Kawata. 2005. Amyloid fibril formation of alpha-synuclein is accelerated by preformed amyloid seeds of other proteins: implications for the mechanism of transmissible conformational diseases. *J. Biol. Chem.* 280:38609–38616.

44. Lorenzen, N., S. I. Cohen, ..., D. Otzen. 2012. Role of elongation and secondary pathways in S6 amyloid fibril growth. *Biophys. J.* 102:2167–2175.

45. White, D. A., A. K. Buell, ..., C. M. Dobson. 2010. Protein aggregation in crowded environments. *J. Am. Chem. Soc.* 132:5170–5175.

46. Chen, E., A. Christiansen, ..., P. Wittung-Stafshede. 2012. Effects of macromolecular crowding on burst phase kinetics of cytochrome c folding. *Biochemistry.* 51:9836–9845.

47. Werner, T. E. R., I. Horvath, and P. Wittung-Stafshede. 2021. Response to crowded conditions reveals compact nucleus for amyloid formation of folded protein. *QRB Discovery.* 2:e2.

48. Arosio, P., T. P. Knowles, and S. Linse. 2015. On the lag phase in amyloid fibril formation. *Phys. Chem. Chem. Phys.* 17:7606–7618.

49. Törnquist, M., T. C. T. Michaels, ..., S. Linse. 2018. Secondary nucleation in amyloid formation. *Chem. Commun. (Camb.).* 54:8667–8684.

50. Cohen, S. I., M. Vendruscolo, ..., T. P. Knowles. 2011. Nucleated polymerization with secondary pathways. I. Time evolution of the principal moments. *J. Chem. Phys.* 135:065105.

51. Knowles, T. P., C. A. Waudby, ..., C. M. Dobson. 2009. An analytical solution to the kinetics of breakable filament assembly. *Science.* 326:1533–1537.

52. Mourão, M. A., J. B. Hakim, and S. Schnell. 2014. Connecting the dots: the effects of macromolecular crowding on cell physiology. *Biophys. J.* 107:2761–2766.